Analysis and Design of a 3-Coil Wireless Power Transmission System for Biomedical Applications

Manjunath Machnoor, *Student Member, IEEE*, Erik Saturnino Gámez Rodríguez, *Member, IEEE*, Pragya Kosta, *Student Member, IEEE*, John Stang, *Member, IEEE*, and Gianluca Lazzi, *Fellow, IEEE*

***Abstract*— Wireless power transfer is a practical and widely used method to power various implantable devices. Commonly, the implanted receiver (RX) must be small, often on the order of millimeter, which poses significant design challenges. In this paper, a technique to improve the performance of systems with a size (inductance)-limited implanted RX coil is explored. Conventionally, only mutual coupling between coils is used to optimize the performance, which constrains the layout/geometry and choice of coils. In the proposed system, mutual coupling, mutual capacitance, and relative polarity can all be used, thereby reducing the constraints on coil layouts. Performance is further enhanced by two additional techniques that maximize the reflected impedance between the RX coils. Three designs (two-coil, conventional three-coil, and the proposed three-coil) are implemented with a 35 mm diameter RX coil, and their performance is measured at 5 MHz with a 1 kΩ load resistance. The efficiency of these designs is measured at varying distances (20–60 mm) between the transmitter and RX. The efficiency of the proposed three-coil system at 50 mm separation is 40%, while the implemented conventional three-coil system and the two-coil system are each less than 10%. Finally, the advantage of the proposed strategy in terms of RX coil current and load tolerance is discussed.**

***Index Terms*— Biomedical implants, coil polarity, dot convention, efficiency, load tolerance, mutual capacitance, mutual coupling, PTE, secondary current, three-coil WPT system, wireless power transfer (WPT).**

I. Introduction

PROGRESS in biomedical implants has enabled, in recent years, unprecedented devices for health monitoring, treatments of diseases, and prosthetics. Advances in enabling technology for implants (semiconductor industry, packaging, biocompatible materials, and so on) have played a significant role in rapidly expanding the development and adoption of biomedical implantable devices. With this growth, wireless power transfer (WPT) has become a critical enabling component since implants must often be charged from devices outside the human body. WPT removes the need for implantable batteries or cabling requirements, making biomedical implants more practical [1], [2]. Besides biomedical implants [3]–[7], WPT has found application in the fields of electric vehicles battery charging [8]–[11] and communication [12], [13] to name a few, with more applications rapidly emerging thanks to the appeal of charging wirelessly and conveniently.

WPT is commonly implemented using two inductively coupled coils/antennas [1]. In WPT systems, a capacitor is generally used to reduce the reactive power stored in the system by compensating for the inductive coil reactance [14], [15]. The reactance does not contribute to power transfer, and therefore, reducing it leads to a better power factor in the system [9]. Improved coupling and load tolerance is often achieved using more than two inductive coils/antennas [3]–[6], [16], and impedance matching of the load [7], [17]–[21] is employed extensively. Load matching can be achieved using additional passive/active components [7], [17]–[21] or using three-coil or four-coil systems [3]–[6], [22], [23]. The ultimate goal of the WPT system is to achieve the required power transfer to a given load with maximum efficiency [24], [25].

WPT systems for biomedical implants have additional constraints: they must comply with electromagnetic safety standards [such as that of complying with the maximum allowable specific absorption rate (SAR) [26]]; they must be biocompatible; and they have often specific longevity requirements [27]–[30]. Both the two-coil [7], [17], [31] and three-coil [4] designs have been successfully employed in biomedical applications: the advantages of using a three-coil system over a two-coil system are generally better misalignment insensitivity, coupling enhancement, lower induced fields in the body, and better bandwidth [3], [4], [10], [32], [33].

The size of the WPT system for biomedical implants is a critical design variable, as the available area is often very limited [34]–[36]. In addition, it has been demonstrated that a larger size increases the risk of tissue inflammation, cell damage [37], [38], and discomfort to the patient. These challenges associated with the design of WPT systems for biomedical implants are the primary motivation of this paper.

Summarizing, the overall design goals of WPT for biomedical implants and, therefore, the goals considered in this paper are: small size (inductance) of the coil implanted in the body ($Goal_1$), low loss in the receiver (RX) ($Goal_2$), and

Manuscript received March 29, 2018; revised August 27, 2018; accepted September 30, 2018. Date of publication November 28, 2018; date of current version August 12, 2019. This work was supported by Research to Prevent Blindness, New York, NY, USA, through an UNRESTRICTED GRANT to the Department of Ophthalmology. *(Corresponding author: Manjunath Machnoor.)*

M. Machnoor, J. Stang, and G. Lazzi are with the Department of Electrical Engineering, University of Southern California, Los Angeles, CA 90007 USA (e-mail: machnoor@usc.edu).

E. S. Gámez Rodríguez and P. Kosta are with the Department of Electrical and Computer Engineering, The University of Utah, Salt Lake City, UT 84112 USA.

Color versions of one or more of the figures in this paper are available online at http://ieeexplore.ieee.org.

Digital Object Identifier 10.1109/TAP.2018.2883687

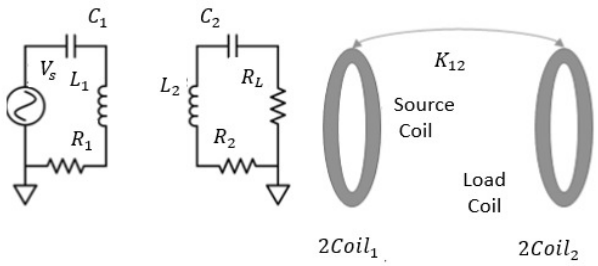

Fig. 1. Schematic of a traditional two-coil WPT system.

high efficiency and power delivery. There are several popular designs of WPT systems for biomedical implants available in the literature [3], [4], [6]. To effectively achieve the stated goals in a three-coil WPT system, circuit-theory based design strategies are discussed in this paper. The performance of the designs in [3] and [4], which have two coils implanted in the body, will be compared with the systems devised through the design strategies outlined here. In order to pursue the best load matching, in this paper, we employ two additional degrees of freedom to maximize the reflected impedance for a given RX coil size (inductance): 1) the relative voltage polarity of the two RX coils (given by dot convention) and 2) a mutual capacitor C_m [which in addition to improving the system performance by reducing the complex power, is also used to tune and match the impedance of the RX for maximum power transfer (MPT)]. This simplifies the design process of the three-coil WPT systems significantly since optimizing the number of turns of the receiving coil is not required.

A brief analysis of the conventional two-coil and three-coil system is presented in Section II. Performance degradation of the conventional two-coil and three-coil system with reduction in RX size is analyzed in Section III. A modified three-coil system is analyzed in Section IV. Sections V and VI build on the three-coil system version of Section IV and adopt two additional circuit design techniques to achieve Goals 1 and 2, respectively. Additional advantages of the considered implementation of the modified three-coil system are mentioned in Section VII. Section VIII provides the experimental verification of the results. Discussion on the biological tissues and other typologies of the multicoil system is presented in Section IX.

II. Brief Notes on Conventional Two-Coil and Three-Coil Wireless Power Transfer Systems

A. Conventional Two-Coil WPT System

A conventional two-coil ($2Coil$) WPT system consists of two inductively coupled coils, one connected to the transmitter (TX) and another to the RX. The coupling coefficient K_{12} of the two coils indicates the ratio of the magnetic field density in the load ($2Coil_2$) and transmit ($2Coil_1$) coils; a schematic view of the system with a power source at the TX, load at the RX, and compensating capacitors [in the resonance condition, expressed by (1)], is shown in Fig. 1. The theory of a $2Coil$ WPT system can be explained using matrix theory and reflected impedance theory [3]–[6]. Kirchhoff's voltage law (KVL) equations for the $2Coil$ system can be written in matrix form, as shown in (2). The determinant of the impedance matrix Z, when expressed in canonical form, can be used to obtain the reflected impedance from $2Coil_2$ to $2Coil_1$, as shown in (5). Compared with the explanation offered in [3]–[6], the various impedances of the system can be derived from the determinant of the matrix, and the system performance is analyzed using the matrix theory. Following the approach in [3]–[6], we can write (1)–(6), where R_1 is the parasitic resistance of $2Coil_1$, R_2 is the parasitic resistance of $2Coil_2$, R_{ref} is the reflected impedance from $2Coil_2$ to $2Coil_1$, $L_{12} = K_{12}\sqrt{L_1 L_2}$ is the mutual inductance between the coils, and i_1 andi_2 are the currents flowing through $2Coil_1$ and $2Coil_2$, respectively.

The performance parameters of the design considered in this paper are: 1) power delivered to the load (PDL) and 2) power transfer efficiency (PTE) η, which is defined as the ratio of PDL to input power under resonance condition. The reflected impedance parameters are used to define PTE and PDL and analyze the effect of the parameters on design goals ($Goal_1$ and $Goal_2$). For the $2Coil$ system, η is given by (4) [3]–[6]

$$\frac{1}{j\omega C_1} = j\omega L_1, \quad \frac{1}{j\omega C_2} = j\omega L_2 \tag{1}$$

$$V = Z \times I \tag{2}$$

$$\begin{bmatrix} V_s \\ 0 \end{bmatrix} = \begin{bmatrix} R_1 & j\omega L_{12} \\ j\omega L_{12} & R_2 + R_L \end{bmatrix} \begin{bmatrix} i_1 \\ i_2 \end{bmatrix} \tag{3}$$

$$det(Z) = Z_1 \times Z_2, \quad Z_1 = R_1 + R_{ref}, \; Z_2 = R_2 + R_L \tag{4}$$

$$R_{ref} = \frac{w^2 L_{12}^2}{R_2 + R_L} \tag{5}$$

$$\eta_{2coil} = \frac{|i_2|^2 R_L}{V_s |i_1|}. \tag{6}$$

Cramer's rule can be applied to solve the impedance matrix equation [see (5)] to find the values of i_1 and i_2. Equation (6) can be written in terms of reflected impedance R_{ref}, as follows:

$$\eta_{2coil} = \frac{R_{ref}}{R_1 + R_{ref}} \frac{R_L}{R_2 + R_L}. \tag{7}$$

The total system PTE of $2Coil$ can therefore be expressed as a product of two terms: PTE of $2Coil_1(\eta_{2coil_1})$ and PTE of $2Coil_2(\eta_{2coil_2})$, as given by (8) [3]–[6]

$$\eta_{2coil} = \eta_{2coil_1} \times \eta_{2coil_2}. \tag{8}$$

Similarly, the definition of PDL for the $2Coil$ system can be expressed in terms of R_{ref} [3]–[6]

$$PDL_{2coil} = P_{in} \times \eta_{2coil} \tag{9}$$

$$PDL_{2coil} = V_s^2 \frac{R_{ref}}{(R_1 + R_{ref})^2} \frac{R_L}{R_2 + R_L}. \tag{10}$$

PDL can also be calculated by measuring the gain (V_{out}/V_{in}) of the system from two-port network parameters [3], [6]. Given that the quality factor of the coils in Fig. 1 can be written as $Q_1 = (\omega L_1/R_1)$ and $Q_2 = (\omega L_2/R_2 + R_L)$, substituting Q_1, Q_2 and $L_{12} = K_{12}\sqrt{L_1 L_2}$ in η_{2coil}, (5) can be rewritten in a form similar to [3]–[6]

$$\eta_{2coil} = \frac{K_{12}^2 Q_1 Q_2}{1 + K_{12}^2 Q_1 Q_2} \frac{R_L}{R_2 + R_L}. \tag{11}$$

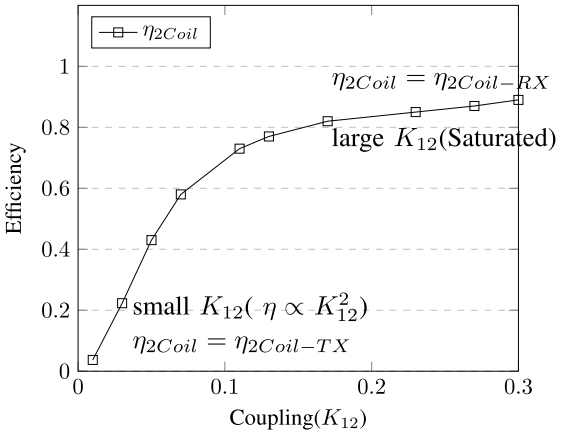

Fig. 2. η_{2Coil} versus K_{12} for the 2-coil system with $L_1 = L_2 = 2$ μH, $R_1 = R_2 = 1$ Ω, RL = 100 Ω, and $f = 5$ MHz.

The following observations about the two-coil system can be made with specific consideration to biomedical applications.

1) If $R_L \gg R_2$, η_{2coil_2} is close to unity and no power is dissipated in the RX coil of the system. This ensures that the power loss in the RX coils implanted in the body is negligible. This condition also reduces PDL.
2) Since R_{ref} is inversely proportional to R_L [see (5)], a higher value of R_L (which ensures higher η_{2coil_2}) reduces η_{2coil_1}. This results in poor η_{2coil} and increased power loss in the $2Coil_1$. This issue can be resolved using the three-coil system and is addressed in Section II-B.
3) The coupling coefficient K_{12} is a function of the dimensions of $2Coil_2$ and $2Coil_1$.

Fig. 2 shows the plot of η_{2Coil} as a function of K_{12} for a typical embodiment of a two-coil WPT system characterized by $L_1 = L_2 = 2$ μH, $R_1 = R_2 = 1$ Ω, $R_L = 100$ Ω, and $f = 5$ MHz. The PTE(η) versus K_{12} plot for a typical WPT has the similar trend. Noting that $2Coil_1$ is the TX and $2Coil_2$ is the RX, we can write that $\eta_{2Coil_1} = \eta_{2Coil_{TX}}$ and $\eta_{2Coil_2} = \eta_{2Coil_{RX}}$. In the design of a $2Coil$ system, $\eta_{2Coil_{RX}}$ is constant and does not vary with the distance between the coils, and it is $\eta_{2Coil_{TX}}$, which varies with the distance between the coils. From Fig. 2, it can be concluded that the RX efficiency (implanted coil $2Coil_2$) can be thought of as the saturation efficiency at high K_{12} (which is found for small distances between coils). The efficiency of the system at low K_{12} is limited by $\eta_{2Coil_{TX}}$, which has square dependence on K_{12} for low K_{12} values.

The secondary side of the two-coil system can also be connected in parallel. The efficiency of secondary of the parallel connected coil is given by [39]

$$\eta_{2Coil_2-Parallel} = \frac{R_L}{R_L + R_s + \frac{R_s R_L^2}{\omega^2 L_2^2}}$$

$$\eta_{2Coil_2-Series} = \frac{R_L}{R_L + R_s}.$$

As L_2 becomes small, which is typical for a biomedical implant, for a given $\omega \& R_L$, $\eta_{2Coil_2(Parallel)}$ is severely limited [39]. Parallel resonance secondary has better reflected impedance compared with the series connected RX, but its RX efficiency is limited. For example, for the $2Coil$ system design considered in this paper, $L_2 = 1$ μH, $R_2 = 0.5$ Ω, $f = 5$ MHz, and $\eta_{2Coil_2(Parallel)} = 0.56$, whereas $\eta_{2Coil_2(Series)} = 0.99$. For this reason, in this paper, the series resonance configuration of the secondary for the two-coil system is considered, and its overall efficiency is improved using the three-coil system.

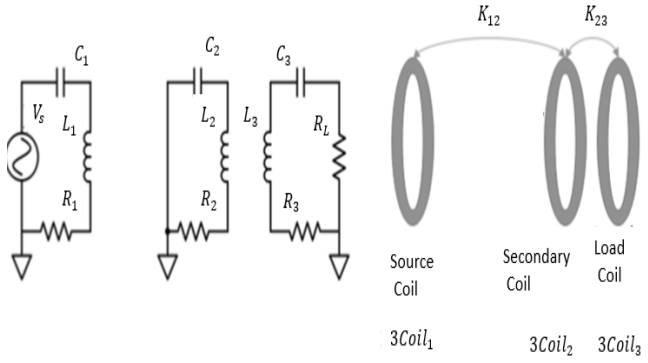

Fig. 3. Schematic of a conventional three-coil WPT system ($3Coil$) [3]–[6].

B. Three-Coil WPT System

A three-coil ($3Coil$) WPT system consists of three inductively coupled coils; one coil is connected to the TX, and two coils are used at the RX end [4]. The coupling coefficients (K_{12} and K_{23}) and the physical layout and schematic are shown in Fig. 3. The additional coil used at the RX, termed secondary coil ($3Coil_2$), is responsible for enhancing the PTE of the system under high R_L conditions. The operation of the 3Coil WPT system can be also understood using the matrix theory and reflected impedance theory [3]–[6]. KVL equations for the resonant [see (12)] $3Coil$ system, written in matrix form, lead to the Z matrix whose determinant can be used to obtain the two reflected impedances R_{ref1} and R_{ref2} of the $3Coil$ system, which are given in (13) [10]

$$\frac{1}{j\omega C_1} = j\omega L_1, \quad \frac{1}{j\omega C_2} = j\omega L_2, \quad \frac{1}{j\omega C_3} = j\omega L_3 \tag{12}$$

$$R_{ref1} = \frac{w^2 L_{12}^2}{R_2 + \frac{w^2 L_{23}^2}{R_3 + R_L}}, \quad R_{ref2} = \frac{w^2 L_{23}^2}{R_3 + R_L} \tag{13}$$

where R_1 is the parasitic resistance of $3Coil_1$, R_2 is the parasitic resistance of $3Coil_2$, R_3 is the parasitic resistance of $3Coil_3$. R_{ref1} is the reflected impedance from $3Coil_2$ to $3Coil_1$, and R_{ref2} is the reflected impedance from $3Coil_3$ to $3Coil_2$. The mutual inductances between the coils $L_{12} = K_{12}\sqrt{L_1 L_2}$ and $L_{23} = K_{23}\sqrt{L_2 L_3}$ are the result of the coupling K_{12}, K_{23} between the coils, while i_1, i_2, and i_3 are the currents flowing through $3Coil_1, 3Coil_2$, and $3Coil_3$, respectively. Following a similar analysis to that of the 2 coil system, the equation for the PTE can be written in terms of reflected impedances R_{ref1} and R_{ref2} as follows:

$$\eta_{3coil} = \frac{R_{ref1}}{R_1 + R_{ref1}} \frac{R_{ref2}}{R_2 + R_{ref2}} \frac{R_L}{R_3 + R_L}. \tag{14}$$

The total efficiency of the 3Coil system can be expressed as a product of the efficiencies of $3Coil_1$, $3Coil_2$, and $3Coil_3$, as given by (15)

$$\eta_{3coil} = \eta_{3Coil_1} \times \eta_{3Coil_2} \times \eta_{3coil_3} \tag{15}$$

where η_{3coil_1}, η_{3coil_2}, and η_{3coil_3} are the efficiencies of $3Coil_1$, $3Coil_2$, and $3Coil_3$ respectively. Similarly, the PDL for the $3Coil$ system can be expressed in terms of R_{ref1} and R_{ref2} [3]–[6]

$$PDL_{3Coil} = V_s^2 \frac{R_{ref1}}{(R_1 + R_{ref1})^2} \frac{R_{ref2}}{R_2 + R_{ref2}} \frac{R_L}{R_3 + R_L}. \tag{16}$$

The following observations about the three-coil system can be made with specific consideration to the biomedical applications.

1) If $R_L \gg R_3$, η_{3coil_3} is close to 1, and no power is dissipated in the $3Coil_3$ of the system. However, this does not guarantee that the power loss in the RX coils implanted in the body is minimized. Nonetheless, this condition does not imply sufficiently high PDL.
2) R_{ref2} is directly proportional to L_2 and L_3. High inductance (obtained through the length of $3Coil_2 + 3Coil_3$) results in high R_{ref2} and high η_{3coil_2}. Large R_{ref2} ($> R_2$) and R_L ($> R_3$) are sufficient condition to reduce the power dissipation in the implanted coils of 3Coil.
3) The main functionality of $3Coil_2$ is to invert and scale the contribution of the load coil ($3Coil_3$) on the reflected impedance at $3Coil_1$. Comparing R_{ref} [see (5)] of the $2Coil$ system with R_{ref1} [see (13)] of $3Coil$ system, the above-mentioned functionality of the $3Coil_2$ can be confirmed [i.e., $R_L \longrightarrow (\omega^2 L_{23}^2 / R_L + R_3)$]. This is referred to as the impedance matching capability of the $3Coil$ system.
4) The general plot of η_{3Coil} as a function of K_{12} has the trend as shown in Fig. 2. Noting that $3Coil_1$ is the TX and $3Coil_2$&$3Coil_3$ forms the RX, we can write $\eta_{3Coil_1} = \eta_{3Coil_{TX}}$ and $\eta_{3Coil_2} \times \eta_{3Coil_3} = \eta_{3Coil_{RX}}$.

III. Performance Degradation in Conventional Two-Coil and Three-Coil System as the Receiver Size Reduces

The design of the 3-coil WPT system involves placing the additional secondary coil closer to the coil with low Q [40]. In biomedical applications [4] of the $3Coil$ system, two coils are located at the RX side and one coil is at the TX. As the size of the two RX coils reduces (either in terms of diameter or the number of turns), L_2, L_3, and their mutual inductance L_{23} reduce. This results in reduced R_{ref2}; as a result, η_{3coil_2} [see (14) and (15)] decreases and losses in the implanted coil increase. Furthermore, R_{ref1}, which is inversely proportional to R_{ref2}, either increases or saturates depending on the value of R_{ref2}. The efficiency of the system η_{3coil} will be limited by η_{3coil_2}: since R_{ref2} decreases and R_{ref1} either increases or saturates, PDL_{3coil} [see (16)] also decreases as the size reduces. Thus, as the size of the RX coils in the $3Coil$ decreases, PTE and PDL of the entire system decrease and losses in the implanted coils increase. This provides a challenge to design a system with good PTE and PDL. Similarly, by referring to (5) and (7), PTE and R_{ref} of the $2Coil$ system reduces as the size of $2Coil_2$ (L_2) reduces. It can also be concluded that, for the $3Coil$ system with small RX coils (low L_2 and L_3), performance degradation can be linked to reduction in R_{ref2}. Thus, this paper proposes a technique to maximize R_{ref2} for a three-coil system to achieve good PTE and PDL performance for a small RX three-coil system.

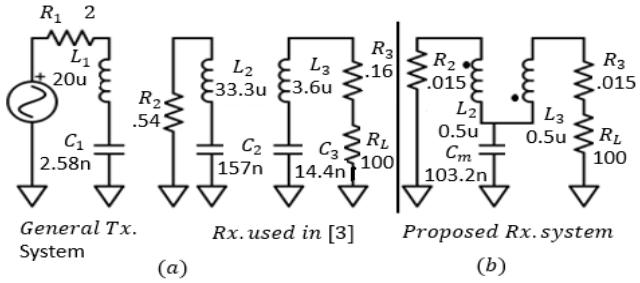

Fig. 4. (a) Schematic of the proposed efficient and compact three-coil system ($3Coil_p$). To maximize R_{ref2} of the small RX size 3-coil system, two techniques are adopted: $L_2 = L_3$ and $(1/\omega C_2) = (1/\omega C_3) = 0$ along with the appropriate RX system's relative coil polarity required to increase R_{ref2p}. (b) RX system's relative coil polarity that leads to the reduction of R_{ref2p}.

The effects of frequency of operation on the human body are explained in [3]. The choice of 700 kHz in [3] and 13 MHz in [4] is made considering the Q-factor of the coils used, following an optimization process. In this paper, we chose the frequency of 5 MHz as the copper wire of AWG 20 exhibited $Q = 150$ for $L = 5$ μH. We have also considered a load resistance $R_L = 1$ kΩ. In this paper, and unlike [3], no further optimization of coils was undertaken to choose a frequency with higher Q as high Q is not necessary to obtain higher PTE with the approach presented here.

There is no established standard for the design of WPT systems for biomedical implants but the general designs in the literature include TX coil larger than the implanted RX coil with dimensions in tens of millimeter [3]–[6], [26], [41]. The biomedical implant systems are generally designed to efficiently deliver power of the order of 100 mW (50–300 mW) to the RX [4].

IV. Enhancing the Performance of Three-Coil System as the Receiver Size Reduces

The resonant condition for the conventional three-coil system [3]–[6] is provided in (12). In this paper, we consider a different resonant condition: while the layout of the proposed three-coil system ($3Coil_p$) remains the same as Fig. 3, the resonance condition is changed to (17) instead of (12). This results in a new schematic equivalent of the $3Coil_p$ system shown in Fig. 4 (note that the dot convention is used to denote the voltage polarity of the coils).

The advantage of this system is understood using the matrix theory and reflected impedance theory [3]–[6]. The impedance matrix equation for the modified resonant scheme is provided in (18): compared with the Z matrix of the conventional $3Coil$ [3]–[6], the Z matrix of $3Coil_p$ [see (18)] includes the impedance of the capacitor C_m used for creating a resonance

condition at the RX coils. From the determinant of the resonant Z matrix (impedance matrix) when expressed in the canonical form, we can obtain the two reflected impedances R_{ref1p} and R_{ref2p} for the proposed three-coil system $3Coil_p$ [see (18)]. The main advantage of this system is that it increases the effective mutual impedance between the $3Coil_{2p}$ and $3Coil_{3p}$; the equivalent L_{23p} of the system increases, as shown in (21). Since we have noted in Section III that, as the size of the RX in the three-coil system reduces, R_{ref2} reduces, adopting this new resonant condition helps us maximize R_{ref2} of the small RX in the three-coil system. By increasing R_{ref2p}, the PTE and PDL can be increased, and the losses in the implanted coil can be reduced. Both three-coil systems under consideration ($3Coil$ and $3Coil_p$) have the same set of variables to describe the operation; in order to differentiate the variables of the two systems, the proposed three-coil system uses subscript $_p$ for all the variables (for example, R_{ref2} is for the $3Coil$ system and R_{ref2p} is for the $3Coil_p$ system)

$$\frac{1}{j\omega C_1} = j\omega L_1, \quad \frac{1}{j\omega C_m}+\frac{1}{j\omega C_2} = j\omega L_2$$
$$\frac{1}{j\omega C_m}+\frac{1}{j\omega C_3} = j\omega L_3 \tag{17}$$

$$V = Z \times I \tag{18}$$

$$\begin{bmatrix} V_s \\ 0 \\ 0 \end{bmatrix} = \begin{bmatrix} R_1 & j\omega L_{12} & 0 \\ j\omega L_{12} & R_2 & j\omega L_{23} - \dfrac{1}{j\omega C_m} \\ 0 & j\omega L_{23} - \dfrac{1}{j\omega C_m} & R_3+R_L \end{bmatrix} \times \begin{bmatrix} i_1 \\ i_2 \\ i_3 \end{bmatrix} \tag{19}$$

$$j\omega L_{23} \longrightarrow j\left(\omega L_{23}+\frac{1}{\omega C_m}\right) \tag{20}$$

$$det(Z) = Z_1 \times Z_2 \times Z_3 \tag{21}$$

$$Z_1 = R_1+R_{ref1p}, \quad Z_2 = R_2+R_{ref2p}, \quad Z_3 = R_3+R_L$$

$$R_{ref1p} = \frac{\omega^2 L_{12}^2}{R_2+\frac{\left(\omega L_{23}+\frac{1}{\omega C_m}\right)^2}{R_3+R_L}}, \quad R_{ref2p} = \frac{\left(\omega L_{23}+\frac{1}{\omega C_m}\right)^2}{R_3+R_L}. \tag{22}$$

In (18), R_1 is the parasitic resistance of $3Coil_{1p}$, R_2 is the parasitic resistance of $3Coil_{2p}$, and R_3 is the parasitic resistance of $3Coil_{3p}$. R_{ref1p} is the reflected impedance from $3Coil_{2p}$ to $3Coil_{1p}$, and R_{ref2p} is the reflected impedance from $3Coil_{3p}$ to $3Coil_{2p}$. R_L is, instead, the load resistance. Following the analysis of the η_{3Coil} system, PTE and PDL for the η_{3Coil_p} system can be defined as in (14)–(16) with an updated definition of R_{ref2p}. The notation $_p$ is adapted for the proposed system; $\eta_{3coil_{1p}}$, $\eta_{3coil_{2p}}$, and $\eta_{3coil_{3p}}$ are the efficiency of $3Coil_{1p}$, $3Coil_{2p}$, and $3Coil_{2p}$, respectively.

For the proposed three-coil ($3coil_p$) system, we can make the following observations.

1) If $R_L \gg R_3$, $\eta_{3coil_{3p}}$ is close to 1, and no power is dissipated in the load coil of the system. However, this does not guarantee that power loss in the secondary ($3coil_{2p}$) coil implanted in the body is minimized.
2) It is worth noting that R_{ref1p} and R_{ref2p} of the $3Coil_p$ system in (22) are different from those in (13). ωC_m, which helps increase R_{ref2p}, results in the decrease of R_{ref1p}. A decrease of R_{ref1p} will result in the reduction of $\eta_{3Coil_{1p}}$. That is, mutual capacitor at the RX reduces the efficiency of $3Coil_{1p}$, which is used at the TX. This calls for the efficient design of transmit coil. This issue is addressed in Section VI.
3) In the conventional three-coil ($3Coil$) system, only the mutual impedance between the two RX coils was used for the determination of R_{ref2} and the PTE and PDL of the three-coil system [see (13)]. In the proposed three-coil ($3Coil_p$) system, all the impedances of the RX contribute to R_{ref2p} [see (23)], PTE, and PDL. This effectively enhances the reflected impedance for a given RX system, enabling a smaller and more compact design

$$R_{ref2p} = \frac{\omega^2 L_{23}^2 + \frac{1}{\omega^2 C_m^2} + \omega^2 L_2 L_{23} + \omega^2 L_3 L_{23}}{R_3 + R_L}. \tag{23}$$

As can be noted from (23), L_2, L_3, C_m, and L_m contribute (if $(1/C_m) = \omega^2 L_2 = \omega^2 L_3$) to R_{ref2p} of the $3Coil_p$ system. This leads to the effective utilization of all the impedance sources implanted in the body.
4) It should be noted that the relative polarity of the proposed three-coil ($3Coil_p$) system (that is, the order of connected ends of the inductors) now becomes more important compared with the conventional $3Coil$ system. If the coils are reversed [as indicated by the adjusted dot locations in Fig. 4(b)], then R_{ref2p} reduces like in (24) instead of increasing like in (22). Therefore, coil polarity should be configured as shown in Fig. 4(a) for maximum reflected impedance

$$R_{ref2p} = \frac{\left(\omega L_{23} - \frac{1}{\omega C_m}\right)^2}{R_3 + R_L}. \tag{24}$$

In this paper, two additional circuit techniques are adopted to maximize R_{ref2p} for a given values of L_2 and L_3 and to meet $Goal_1$ and $Goal_2$ of this paper. The first technique is related to splitting the given length of wire as L_2 and L_3 equally, to achieve efficient usage of cable length implanted in the body ($Goal_1$) (covered in Section V). The second circuit technique leads to $(1/\omega C_2) = (1/\omega C_3) = 0$ for the circuit shown in Fig. 4; this also results in higher R_{ref2p} and helps us achieve $Goal_2$ (covered in Section VI).

V. $Goal_1$: Efficient Use of Wire to Enhance R_{ref2} of Smaller Receiver Three-Coil System ($L_2 = L_3$)

A. Circuit Technique Description

It is noted from (13)–(15) that, by using higher L_2 and L_3, we can increase the PTE of the secondary $3Coil_2$ and load coils $3Coil_3$ and reduce the power dissipation in the RX system. However, it is always convenient to use smaller implant and shorter wire inside the human body. Although the inductance that can be achieved for a coil depends on the process used to make the inductor, on a first approximation,

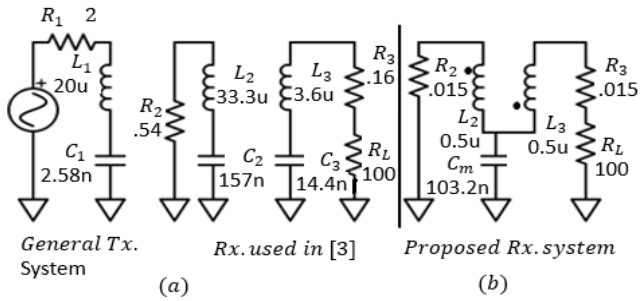

Fig. 5. (a) Equivalent schematic of the system used in [3] ($K_{23} = 0.62$). (b) Proposed RX system incorporating the equal split inductance ($K_{23p} = 0.84$) along with mutual capacitance and appropriate relative polarity. The two RX systems shown in this figure are compared using the same TX system (left).

we can consider that the inductance of the coil is proportional to the length of the wire. The coupling between two implanted coils K_{23} of the three-coil system is a function of the diameter of coils; to maximize K_{23}, diameters of two coils must be equal. Although, in this paper, a diameter of 35 mm has been chosen for the implanted coils to compare with other reported biomedical WPT systems [3], [4], [6], the proposed technique is independent of the diameter of the coils used.

Given a chosen length of coil (fixed maximum inductance, L_{max}), the procedure can be summarized as follows:

$$L_2 + L_3 = L_{max}$$
$$maximize\ R_{ref2} = \frac{\omega^2 L_{23}^2}{R_3 + R_L} = \frac{\omega^2 K_{23}^2 L_2 L_3}{R_3 + R_L}$$

that is

$$maximize\ L_2 \times L_3, \quad Solution:\ L_2 = L_3 = \frac{L_{max}}{2}.$$

The maximum reflected impedance from the RX is obtained when the inductances L_2 and L_3 are equal.

B. Testing the Technique: Comparison 1

As a first test, the implanted coils presented in [3] are considered here. In [3], to enhance the efficiency of the implanted coils (to increase R_{ref2}), higher L_2, L_3, and Q_2 at low frequency (700 kHz) are used. An optimization procedure was considered in [3] to find the values of the implanted coil parameters. The equivalent circuit diagram of the two implanted coils in [3] is shown in Fig. 5(a) (note that $Q_2 = (\omega L_2/R_2) = 273$). Reference [3] uses two implanted coils of smaller diameter (and multilayer) but very high secondary coil inductance (L_2) and low load coil inductance (L_3). Since, in this example, only the efficiency of the implanted RX coils ($3Coil_{p2}$ and $3Coil_{p3}$) is compared, choice of the TX coil does not affect the PTE and PDL comparison. Hence, for comparison purpose, a 20 μH TX is used in Fig. 5. It should also be noted that, while the efficient use of wires implanted inside the body was not the design requirement in [3], the resulting system is characterized by a larger inductance of the implanted coil of 36 μH, with a corresponding longer wire. The RX system of [3] [reproduced here as Fig. 5(a)] is compared against the smaller RX system as shown in Fig. 5(b) (note that $Q_{2p} = 145$). The TX used in this smaller RX design is the same; Q_2 of this system is smaller by 45%, and the values of L_2 and L_3 are about 10% of the values used in Fig. 5(a). Both the circuits are compared at the same frequency and load and TX conditions. The PTE, PDL, and frequency response of the two systems under comparison are shown in Figs. 6 and 7, respectively. It can be concluded that, though L_2, L_3, and Q_2 of Fig. 5(b) are smaller than Fig. 5(a), it achieves the same PDL, PTE and frequency performances. This is because of maximization of R_{ref2} achieved using $L_2 = L_3$ and mutual coupling capacitor C_m. This comparison is also summarized in Table I

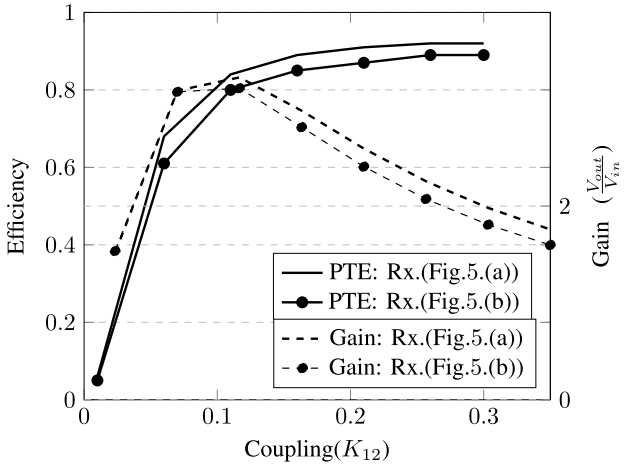

Fig. 6. Comparison of PTE and gain of two systems in Fig. 5 [Fig. 5(a) representing [3] and Fig. 5(b) representing smaller and equal split inductance].

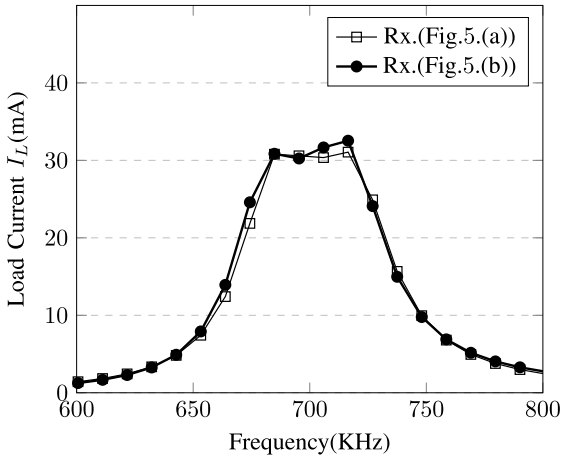

Fig. 7. Comparison of frequency response of load current of two systems in Fig. 5 [Fig. 5(a) representing [3] and Fig. 5(b) representing smaller and equal split inductance].

VI. *Goal*$_2$: Reducing Power Dissipation in the Implanted Receiver (Second Technique to Enhance R_{ref2} of Smaller Receiver 3-Coil System [$(1/\omega C_2) = (1/\omega C_3) = 0$])

A. Circuit Technique Description

The implant coils (RX section) of the conventional three-coil systems have efficiency given by (13)–(15). It can be

TABLE I

RESULTS OF TWO COMPARISON EXERCISES AND THE ADVANTAGES OF THE PROPOSED TECHNIQUES AS COMPARED WITH THE SYSTEMS IN [3] AND [4]

System	η_{RX}	L_2, L_3	Q_2	Comments
[3](Fig.5(a), Rx.only)	0.91	33uH, 3uH	273	Lower L_2, L_3 and Q_2 for a given PTE, PDL and frequency response.
Proposed (Fig.5(b))	0.91	0.5uH, 0.5uH	145	
[4](Fig.8(a))	0.75	0.4uH, 0.4uH	179	C_m increases the receiver efficiency
Proposed (Fig.8(b))	0.96	0.4uH, 0.4uH	179	

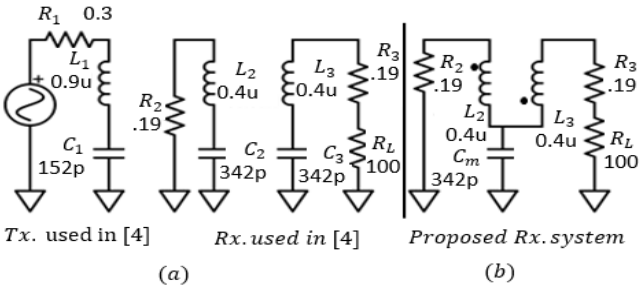

Fig. 8. (a) Equivalent circuit diagram of the system used in [4]. The system is tested for its losses in the RX implanted in the body. (b) Schematic of the proposed RX system. The two RX systems shown in this figure are compared using the same TX System (left).

rewritten as $\eta_{RX_{3coil}}$ as shown in (25). Similarly, $\eta_{RX_{3coilp}}$ is the efficiency of the RX section of the proposed three-coil system, which is given in (26)

$$\eta_{RX_{3coil}} = \frac{\frac{w^2 L_{23}^2}{R_3+R_L}}{R_2 + \frac{w^2 L_{23}^2}{R_3+R_L}} \times \frac{R_L}{R_3+R_L} \tag{25}$$

$$\eta_{RX_{3coilp}} = \frac{\frac{\left(\omega L_{23}+\frac{1}{\omega C_m}\right)^2}{R_3+R_L}}{R_2 + \frac{\left(\omega L_{23}+\frac{1}{\omega C_m}\right)^2}{R_3+R_L}} \times \frac{R_L}{R_3+R_L}. \tag{26}$$

To minimize the losses in the RX system, $\eta_{RX_{3coilp}}$ has to be maximized. To maximize $\eta_{RX_{3coilp}}$, $(1/\omega C_m)$ has to be maximized. This condition leads to $(1/\omega C_2) = (1/\omega C_3) = 0$ in (17) of the proposed three-coil system.

B. Testing the Technique: Comparison 2

As a second test, implanted coils from [4] are considered for the redesign. In [4] (given as L_3 and L_4 for a three-coil system in Table I), a conventional three-coil system is considered for the design. In [4], to enhance the efficiency of the implanted coils (to increase R_{ref2}), higher frequency (13.56 MHz) Q_2 and low L_2 and L_3 are used. The equivalent circuit diagram of the system of [4] is shown in Fig. 8(a). The approach considers two implanted coils of equal inductance (L_2) and (L_3), and the obtained RX efficiency is 0.75. The goal of this section is to increase this implanted RX efficiency to reduce losses and demonstrate the functionality of mutual capacitance (C_m) in the proposed system.

It is to be noted that neither the reduction of power dissipation of the coils implanted in the body nor the efficient usage

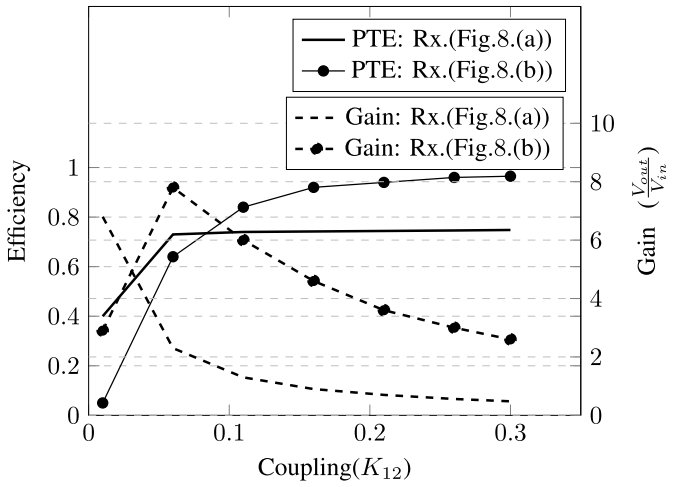

Fig. 9. Comparison of PTE and gain of systems using two different RX configurations in Fig. 8 [Fig. 8(a) representing [4] and Fig. 8(b) representing C_m enhanced system].

of coils implanted in the body was the design requirement in [3]. As a result, $K_{23} = 0.19$ is chosen to reduce R_{ref_2}. This design choice may increase η_{3Coil_1}, although this may come at the expense of higher power dissipation in the body; the resulting system in [4], albeit an efficient one, has 25% of the constant loss in the coils implanted in the body.

The RX system of Fig. 8(a) is compared against the RX system, as shown in Fig. 8(b). The coils used in this design are the same; the only difference is that a resonant scheme with $(1/\omega C_2) = (1/\omega C_3) = 0$ [see (17)] is used to minimize the losses of the implanted system. Both the circuits are compared at the same frequency and load and TX conditions. The PTE and PDL (gain) of the two systems are shown in Fig. 9.

The plots of PTE (see Fig. 9) of the two systems [Fig. 8(a) representing [4] and Fig. 8(b) representing $(1/\omega C_2) = (1/\omega C_3) = 0$] under consideration indicate that, the RX efficiency of the system [see Fig. 8(b)] with mutual capacitance is 0.95, while the RX efficiency of the system without mutual capacitance is 0.75. The TX efficiency of the RX enhanced system is reduced [see Fig. 9] but can be increased by increasing the mutual impedance with the TX. The plots of PDL (gain) [see Fig. 9] of the two systems under consideration indicate the advantages of the system [see Fig. 8(b)] with mutual capacitance at the RX at higher K_{12}. This comparison is also summarized in Table I.

VII. DESIGN PROCEDURE AND ADVANTAGES OF THE PROPOSED THREE-COIL SYSTEM OVER CONVENTIONAL 3 COIL SYSTEM

A. Design Procedure

This paper introduces two circuit concepts to enhance the system performance in the proposed three-coil system $3Coil_p$. The equal split of two coils at the RX and common capacitor enhances the reflected impedance of the RX, which enables an efficient WPT for small RXs. This results in efficient use of wires in the body and reduces the power dissipation of the coils in the RX.

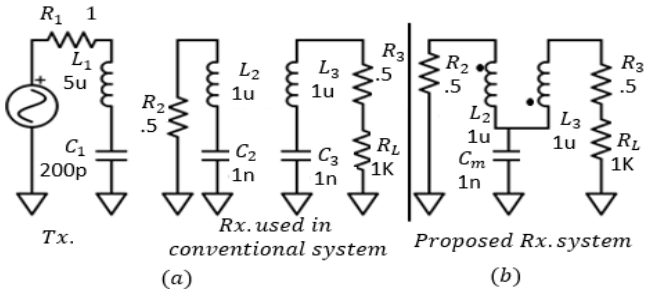

Fig. 10. (a) Schematic of the implemented conventional three-coil system. (b) Schematic of the implemented proposed three-coil system. The two RX systems shown in this figure are compared using the same TX system (left).

The proposed design procedure begins with the observation in [40] that, to increase the efficiency of the three-coil system, I_1, I_2 need to be reduced for given I_3. That is, both (I_1/I_3) and (I_2/I_3) should be minimized. The term (I_1/I_3) relates to the efficiency of the TX, and the term (I_2/I_3) relates to the efficiency of the RX. The conventional and the proposed three-coil systems have the following ratios:

$$\frac{I_1}{I_3} = \frac{R_2(R_3+R_L)+(\omega M_{23})^2}{\omega M_{12}(\omega M_{23})}, \quad \frac{I_2}{I_3} = \frac{(R_3+R_L)}{j\omega M_{23}} \tag{27}$$

$$\frac{I_{1p}}{I_{3p}} = \frac{R_2(R_3+R_L)+\left(\omega M_{23}+\frac{1}{\omega C_m}\right)^2}{\omega M_{12}\left(\omega M_{23}+\frac{1}{j\omega C_m}\right)}$$

$$\frac{I_{2p}}{I_{3p}} = \frac{(R_3+R_L)}{j\omega M_{23}+\frac{1}{j\omega C_m}}. \tag{28}$$

We note that, if the smaller RX system is designed with $R_2(R_L+R_3) = 2\ \omega^2\ M_{23}^2$, then (I_1/I_3) remains unchanged if M_{23} is doubled. That is, if the mentioned condition is satisfied, doubling ωM_{23} will not affect the efficiency of the TX. This approximate doubling of ωM_{23} is achieved through the added conductive pathway linking the two RX coils (with the addition of mutual capacitance, C_m).

To demonstrate the operation and advantages of the proposed system, a RX system with limited size (smaller M_{23}) is designed, and then, using the proposed technique, the efficiency of the RX is enhanced without compromising the TX efficiency. As an example, we have considered, $R_L = 1\ \text{k}\Omega$, $R_2 = R_3 = 0.5\ \Omega$, $R_1 = 1\ \Omega$, $L_1 = 5\ \mu\text{H}, L_2 = L_3 = 1\ \mu\text{H}$, $and f = 5$ MHz. This accounts for all the conditions proposed in this paper that is $L_2 = L_3$, $R_L \gg R_3$, $and R_2(R_L+R_3) = 2\ \omega^2\ M_{23}^2$. The condition $R_2(R_L+R_3) = 2\ \omega^2\ M_{23}^2$ leads to the smaller RX system with poor efficiency, which will be enhanced (doubled) using the proposed system with $(1/\omega C_2) = (1/\omega C_3) = 0$ condition. The system [schematic of the proposed RX system shown in Fig. 10(b) and schematic of the conventional system shown in Fig. 10(a)] is implemented experimentally, and the results are provided in the measurements section. The simulation results showing the design approach of reducing (I_2/I_3) by keeping (I_1/I_3) almost fixed is shown in Fig. 11 (it proves that we can increase the RX performance without affecting the TX efficiency).

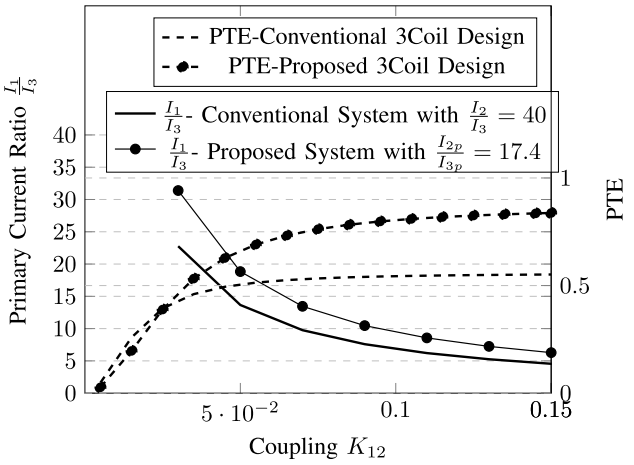

Fig. 11. (I_{2p}/I_{3p}) is lesser than (I_2/I_3) of the conventional system. It proves that we can increase the RX performance without affecting the TX efficiency. At lower K_{12}, PTE is limited by the TX efficiency, which is the same for both the systems.

B. Advantage 1: Tolerance to Load Changes

One of the main advantages of the conventional three-coil system over the two-coil system (parallel secondary) is that its PTE is less sensitive to variation of load. The efficiency of the RX in the proposed three-coil system is less sensitive to load variations compared with the conventional three-coil system. It is to be noted that while the conventional system achieves insensitivity by reducing R_2 [3] (or higher Q2), the proposed system improves the insensitivity by increasing the mutual coupling. The RX efficiency of the conventional and the proposed three-coil systems for the designed parameters is shown in Fig. 12. Following the same analysis, it can be noted that $\eta_{3Coilp-RX}$ is less sensitive to load compared with $\eta_{3Coil-RX}$:

$$\frac{\partial(\eta_{RX-3Coil})}{\partial R_L} = \frac{-\omega^2 M_{23}^2 R_2}{\left(\omega^2 M_{23}^2 + R_2 R_L\right)^2} \tag{29}$$

$$\frac{\partial(\eta_{RX-3Coilp})}{\partial R_L} = \frac{-\left(\omega M_{23}+\frac{1}{\omega C_m}\right)^2 R_2}{\left(\left(\omega M_{23}+\frac{1}{\omega C_m}\right)^2 + R_2 R_L\right)^2}. \tag{30}$$

C. Advantage 2: Reducing Currents in the Secondary Coil

The currents through the intermediate secondary coil of the three-coil system should be reduced for a given load to decrease the losses in the system [40]. The proposed and the conventional systems, for the given design parameters, are evaluated for the secondary coil current for different couplings with the TX coil. The proposed system reduces the current through the secondary coil by enhancing the mutual impedance between the implanted coils, as shown in Fig. 13. The magnetic field is proportional to the current flowing through the coil, and usually, for a single antenna, electric field is proportional to the magnetic field. In the measurements section, it will be shown that the proposed system achieves the

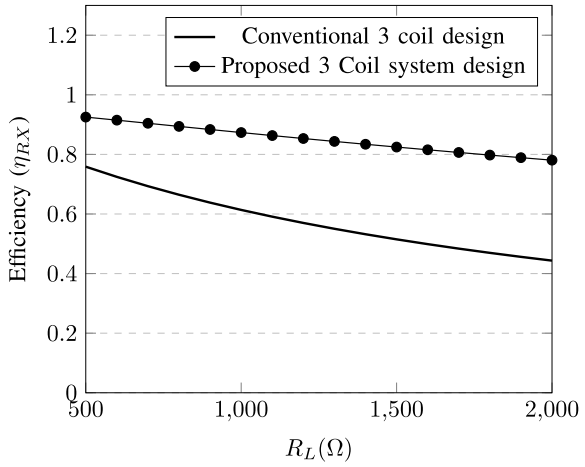

Fig. 12. Comparison of load sensitivity of the efficiency of implanted systems designed using the conventional and the proposed design techniques.

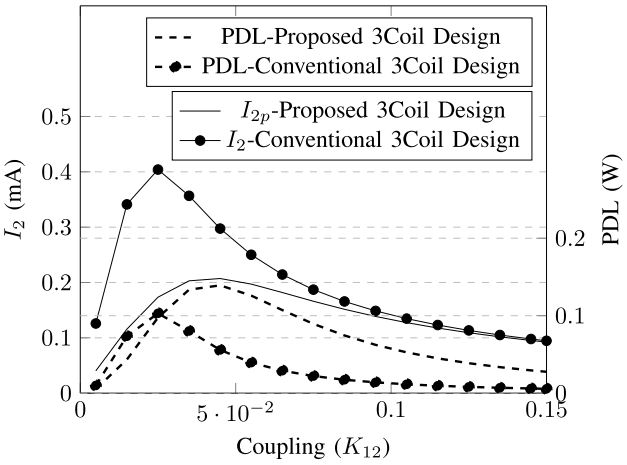

Fig. 13. Comparison of PDL ($V_{in} = 1$) and secondary coil currents of the proposed and conventional designs of the three-coil system. It can be noticed that, for a given PDL, the required value of I_{2p} is less than I_2 for all K_{12}.

same power delivery of the traditional three-coil system while achieving higher efficiency.

D. Load Current I_3 and I_{3p}

The simulated PDL ($I_3^2 R_L$, $I_{3p}^2 R_L$, for $V_{in} = 1$) and current in $Coil_2$ and $Coil_{2p}$ for the conventional three-coil [see Fig. 10(a)] system and the proposed three-coil [see Fig. 10(b)] system for a different K_{12} value are shown in Fig. 13. To analyze the effect of mutual capacitance on the RX currents (I_3, I_2 and I_{3p}, I_{2p}) for the systems under consideration, we solve the matrix in (16) for I_{2p} (similarly for I_2) and rewrite (23) and (24) as (27) (where $R_{3t} = R_3 + R_L$). Thus, it can be noticed in Fig. 13 that at high K_{12} [the terms with ωM_{12} dominate in I_2 (and I_{2p}) and consequently, I_2 becomes equal to I_{2p}], for a given I_2 value (or I_{2p}), the proposed three-coil system has higher load current (I_{3p}) compared with the conventional three-coil system (I_3)

$$I_2 = \frac{j\omega M_{12} R_{3t}}{R_1 R_2 R_{3t} + \omega^2 M_{23}^2 R_1 + \omega^2 M_{12}^2 R_{3t}}$$

$$I_{2p} = \frac{j\omega M_{12} R_{3t}}{R_1 R_2 R_{3t} + \left(\omega M_{23} + \frac{1}{\omega C_m}\right)^2 R_1 + \omega^2 M_{12}^2 R_{3t}}$$

$$I_3 = \frac{I_2\ (j\omega M_{23})}{R_{3t}}, \quad I_{3p} = \frac{I_{2p}\ \left(j\omega M_{23} + \frac{1}{j\omega C_m}\right)}{R_{3t}}. \quad (31)$$

Conversely, for a given load current (fixed $I_3 = I_{3p}$) or PDL, the required value of I_{2p} is less than the required value of I_2 (at lower K_{12}, the terms with ωM_{23} and $\omega M_{23} + (1/\omega C_m)$ dominate in I_2 and I_{2p}, respectively, and $(I_{2p}/I_2) = (\omega M_{23}/\omega M_{23} + (1/\omega C_m))$). This can be attributed to the increased mutual impedance between the $Coil_{2p}$ and $Coil_{3p}$ for the proposed three-coil system.

The maxima of the PDL in Fig. 13 occurs when $R_{ref1} = R_1$ for $3Coil$ and $R_{ref1p} = R_1$ for $3Coil_p$ systems as given by MPT theorem. The PDL maxima for the $3Coil_p$ is higher than the PDL maxima of $3Coil$ and also occurs at slightly higher K_{12}. It is because C_m, which increases R_{ref2}, decreases R_{ref1} slightly. It is to be noted that, this relation is also the consequence of the choice of relative coil polarity.

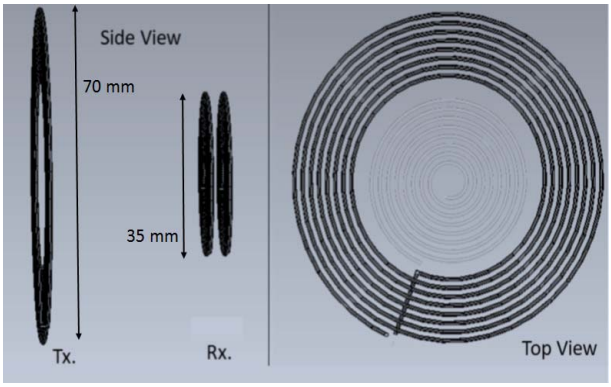

Fig. 14. Layout of the side view and top view of three-coil system in CST Design STUDIO. In the top view, $3Coil_1$ highlighted for differentiation. The diameter of the transmit and receive coils is 70 and 35 mm, respectively.

VIII. Experiments: Measurements and Results

The proposed three-coil system $3Coil_p$ is compared against a conventional three-coil system $3Coil$ and two-coil system $2Coil$. The measurement results are compared against simulation. The side view and top view of the layout of the considered three-coil system is shown in Fig. 14, while the measurement setup is shown in Fig. 15. It is to be recalled that the layout of $3Coil$ and $3Coil_p$ is the same but the resonance condition is different. Two-coil system $2Coil$ is formed by removing the $3Coil_3$ of the $3Coil$ system. The physical and electrical parameters of the coils used in the experiments are shown in Tables II and III, respectively.

In the $3Coil_p$ and $3Coil$ systems, $L_2 = L_3$ is maintained. Furthermore, in the $3Coil_p$ systems, $(1/\omega C_2) = (1/\omega C_3) = 0$ is maintained in the implementation. Finally, in the $3Coil_p$ system, a smaller RX system is designed with $R_2(R_L + R_3) = 2\ \omega^2\ M_{23}^2$, so that (I_1/I_3) remains unchanged if M_{23} is doubled using the proposed design technique. The measurements are performed using a VNA; S-parameters from VNA

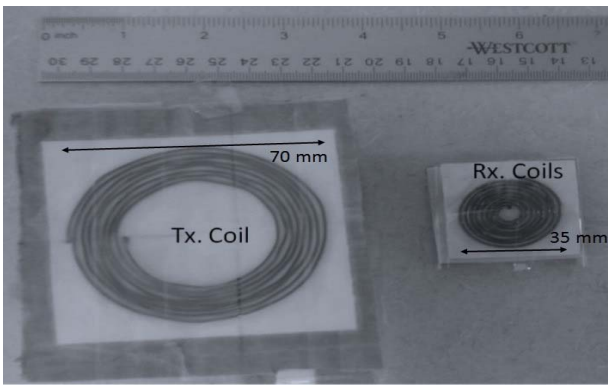

Fig. 15. Photograph of the measurement setup showing TX coil (left) and RX setup (right). The diameter of the transmit and receive coils are 70 and 35 mm, respectively.

TABLE II
PROPERTIES OF THE COILS USED

coil	Coil Diameter(mm)	No. Turns	L(uH)	Q	AWG
Tx.	70	8	5	150	20
Sec.	35	8	1	70	20
Load	35	8	1	70	20

TABLE III
CIRCUIT PARAMETERS OF THREE SYSTEMS UNDER TEST

System	L1(μH)	L2(μH)	L3(μH)	$R_L(k\Omega)$	f(MHz)
2Coil	5	1		1	5
3Coil	5	1	1	1	5
$3Coil_p$	5	1	1	1	5

are converted to Z-Parameters. The performance parameters of interest (PTE [see (32)] and PDL) are expressed using Z-Parameters [3]–[6]. Since it is difficult to measure the exact source voltage (V_s) for VNA measurements, measurement is made independent of V_s by measuring the gain instead. PDL is related to the voltage gain by (33)

$$\eta = \frac{|Z_{21}^2|}{R_L|Z_{11}|cos(Phase(Z_{11}))}, \quad Gain = \frac{|Z_{21}|}{|Z_{11}|} \tag{32}$$

$$PDL = \frac{|V_2^2|}{2R_L} = \frac{|Z_{21}|^2 V_1^2}{2R_L|Z_{11}|^2} = \frac{Gain^2 V_1^2}{2R_L}. \tag{33}$$

The PTE comparison (see Fig. 16) shows that, for a small RX system with large R_L, $\eta_{3Coil_p} > \eta_{3Coil} > \eta_{2Coil}$ for all the distances. Also, η_{3Coil_p} at large distances (small K_{12}) does not fall below $3Coil$. The PTE of the 3Coil at 20 cm separation is 0.4, whereas the PTE of the $3Coil_p$ at 20 cm is 0.8. It can be concluded that, in the considered case, the $3Coil_p$ has double the PTE of $3Coil$. The gain performance (see Fig. 17) of the three-coil system is better than the two-coil system at larger distances for higher loads and smaller coils. The common capacitor circuit ($3Coil_p$) performs better than the conventional three-coil ($3Coil$) system both in terms of efficiency and gain for all the distances between the TX and the RX.

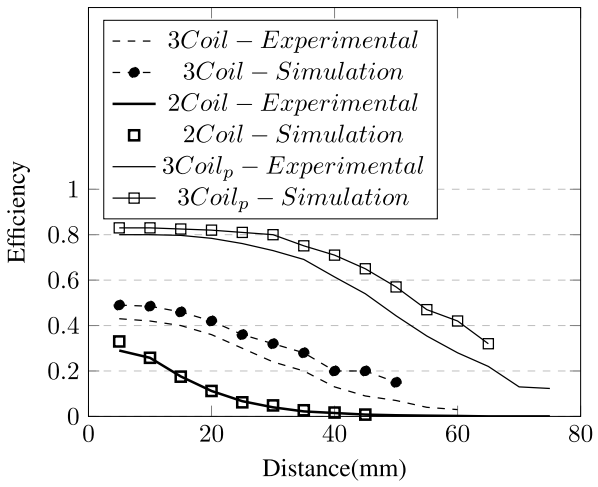

Fig. 16. Experimental and simulation results of PTE of three systems under comparison.

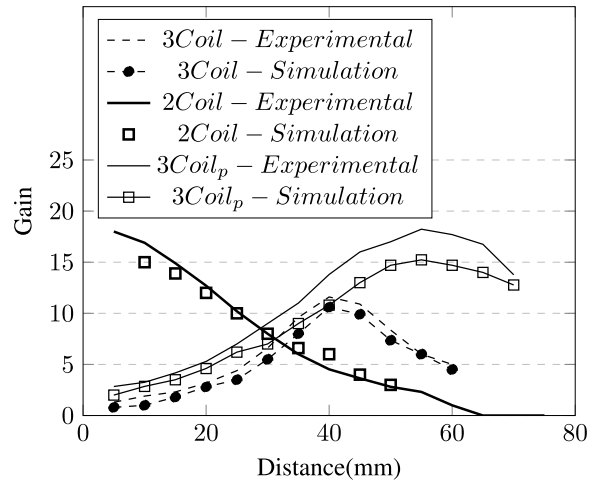

Fig. 17. Experimental and simulation results of gain of three systems under comparison.

IX. DISCUSSION

A. K_{12} and C_m for Optimization of System Performance

In the conventional three-coil ($3Coil$) system, mutual coupling between the two RX coils K_{23} is used to optimize the reflected impedance R_{ref2} to obtain the desired system performance [3]–[6]. The maximization of K_{23} increases the RX efficiency but decreases TX efficiency and vice versa. This dependence of system performance on K_{23} puts a constraint on the coil geometry in the conventional three-coil system. The system in [3] uses a larger (multilayer) secondary coil compared with load coil to achieve K_{23} of 0.6. In the system in [4], additional spacing is used between the two RX coils to achieve a lower K_{23} value of 0.22. These geometries are difficult to implement for a real compact implant RX.

In this proposed three-coil ($3Coil_p$) system, the adopted architectural update leads to new reflected impedance of the secondary R_{ref2p} [see (18)], which not only depends on K_{23} but also on mutual capacitance (C_m) and appropriate relative polarity. Now, C_m have the same effect on the system as K_{23}. This puts less constraints on the K_{23} requirements,

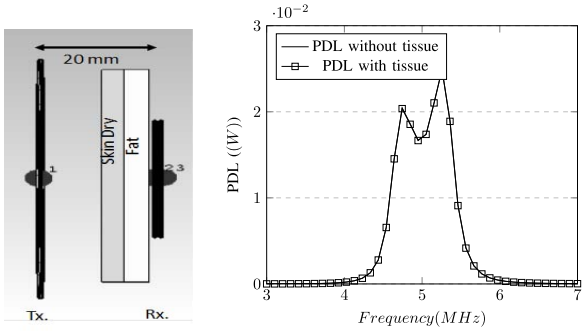

Fig. 18. Study of the effect of tissue material on the system performance. Left: the proposed three-coil WPT system with skin dry (3.75 mm thick) and fat (4 mm thick) tissue in between the TX and the RX. Right: plot of PDL versus frequency for the system with and without the tissue. It can be noted that tissue has no effect on the PDL.

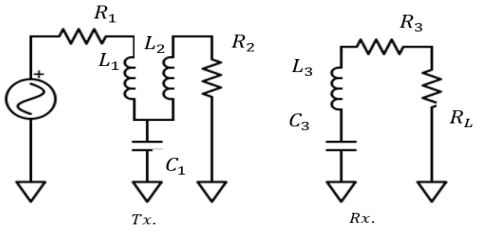

Fig. 19. Schematic of a three-coil system with an additional coil and the mutual capacitor at the TX. The driver coil (L_1) is connected to the TX coil (L_2) using the mutual capacitance (C_1). The choice of relative voltage polarity of L_1 and L_2 (dot convention not shown here) will determine the PTE and PDL.

and we can optimize the layout of the implanted coils to meet additional requirements like smaller size (inductance) or any other variables, like SAR [26], [41] requirements.

In this paper, to demonstrate the advantage of the proposed technique, a RX coil with small inductance is considered. The WPT System designed with the conventional three-coil system approach achieves a RX efficiency of about 41% (η_{RX}) (as can be concluded from Fig. 16 for a distance of 10 mm), whereas, for the same RX coils, the system designed with the proposed three-coil ($3Coil_p$) system approach leads to higher (82%, see Fig. 16) RX efficiency, as the enhancement is obtained by appropriate C_m and relative polarity.

B. Tissue Effects on the System Performance

The proposed WPT system could be used in a cortical implant for vision restoration [26]. In the model of human head, there is a 4 mm of fat and a 3.75 mm of dry skin in between the RX coil and the air interface. To analyze the effects of the human tissue on the proposed system performance, fat and dry skin layers are used in the CST simulation as shown in Fig. 18. The material density, electrical conductivity, and relative permittivity of the materials are presented in [26, Table I]. K_{12}, PTE of the system, is not affected by the tissue, and as a result, the PDL of the system also remains unchanged, as shown in Fig. 18. The PDL of the proposed system for a separation of 20 mm between the TX and the RX at 5 MHz is 18 mW [Gain = 4.25 (see Fig. 17), PDL $= ((V_{in} * Gain)^2/R_L) = ((1 * 4.25)^2/1000)$].

C. Additional Coil at the Transmitter and Four-Coil System

The PTE and PDE are given in the following:

$$PTE = \frac{\frac{\left(\omega M_{12} \pm \frac{1}{\omega C_1}\right)^2}{\frac{\omega^2 M_{23}^2}{R_3+R_L}+R_2}}{\frac{\left(\omega M_{12} \pm \frac{1}{\omega C_1}\right)^2}{\frac{\omega^2 M_{23}^2}{R_3+R_L}+R_2} + R_1} \frac{\frac{\omega^2 M_{23}^2}{R_3+R_L}}{\frac{\omega^2 M_{23}^2}{R_3+R_L} + R_2} \frac{R_L}{R_L+R_3} \tag{34}$$

$$PDL = \frac{V_{in}^2 \frac{\left(\omega M_{12} \pm \frac{1}{\omega C_1}\right)^2}{\frac{\omega^2 M_{23}^2}{R_3+R_L}+R_2}}{\left(\frac{\left(\omega M_{12} \pm \frac{1}{\omega C_1}\right)^2}{\frac{\omega^2 M_{23}^2}{R_3+R_L}+R_2} + R_1\right)^2} \frac{\frac{\omega^2 M_{23}^2}{R_3+R_L}}{\frac{\omega^2 M_{23}^2}{R_3+R_L} + R_2} \frac{R_L}{R_L+R_3} \tag{35}$$

In this paper, a three-coil system with an additional coil at the RX is analyzed. The additional coil of the three-coil system can also be placed at the TX [6]. The schematic of the three-coil system with the additional coil at the TX side is shown in Fig. 19. The effect of the mutual capacitance on the performance parameters PTE [PDL can be analyzed similar to (14)] is analyzed in (35). $(1/\omega C_m)$ can add or subtract to ωM_{12} depending on the relative polarity between the TX and the driver coil. It can be noticed from (35) that, depending on the polarity employed, PDL of the system in Fig. 19 can be enhanced without compromising the PTE [if $(((\omega M_{12} - (1/\omega C_m))^2/(\omega^2 M_{23}^2/R_3 + R_L) + R_2) \gg R_1$] or PTE of the system can be enhanced. Similarly, a four-coil [6] system with the additional coil and mutual capacitance at the TX and the RX can use C_m at the TX to enhance PDL [see (35)] and C_m at the RX to enhance the RX efficiency [see (22)].

X. Conclusion

In this paper, a modified three-coil system configuration is proposed that introduces additional degrees of freedom in the design process. The appropriate relative voltage polarity between coils and the mutual capacitance can now be used in addition to K_{23} in the conventional three-coil systems to control the reflected impedance and hence the system performance. In this design, these additional variables are used to improve the systems with low RX inductance and RX efficiency. Two techniques are considered: 1) equal split of two RX coils in the three-coil WPT system ($L_2 = L_3$) and 2) $(1/\omega C_2) = (1/\omega C_3) = 0$. The combined effect of these concepts leads to a system with high R_{ref2p}. Experiments verify the assertions, with results demonstrating the proposed three-coil system with twice the efficiency of a conventional system for small RX coils. The proposed system design results in a PTE and gain of 0.45 and 15 at 60 mm separation between the TX and the RX at a resonance frequency of 5 MHz and $R_L = 1$ kΩ. In comparison, under the same operating conditions, the conventional three-coil system and two-coil system result in a PTE of less than 0.1 and a gain of less than 5. The proposed system also achieves RX designs with better insensitivity to load variation while also reducing the fields induced in the body due to secondary coil

current. Finally, we show that, at the considered frequency, the system performance is robust to the presence of human tissue.

REFERENCES

[1] R. Bashirullah, "Wireless implants," *IEEE Microw. Mag.*, vol. 11, no. 7, pp. S14–S23, Dec. 2010.

[2] G. Chen, J. Stang, M. Haynes, E. Leuthardt, and M. Moghaddam, "Real-time three-dimensional microwave monitoring of interstitial thermal therapy," *IEEE Trans. Biomed. Eng.*, vol. 65, no. 3, pp. 528–538, Mar. 2018.

[3] A. K. Ram Rakhyani, S. Mirabbasi, and M. Chiao, "Design and optimization of resonance-based efficient wireless power delivery systems for biomedical implants," *IEEE Trans. Biomed. Circuits Syst.*, vol. 5, no. 1, pp. 48–63, Feb. 2011.

[4] M. Kiani, U.-M. Jow, and M. Ghovanloo, "Design and optimization of a 3-coil inductive link for efficient wireless power transmission," *IEEE Trans. Biomed. Circuits Syst.*, vol. 5, no. 6, pp. 579–591, Dec. 2011.

[5] M. Kiani and M. Ghovanloo, "The circuit theory behind coupled-mode magnetic resonance-based wireless power transmission," *IEEE Trans. Circuits Syst. I, Reg. Papers*, vol. 59, no. 9, pp. 2065–2074, Sep. 2012.

[6] A. K. RamRakhyani and G. Lazzi, "On the design of efficient multi-coil telemetry system for biomedical implants," *IEEE Trans. Biomed. Circuits Syst.*, vol. 7, no. 1, pp. 11–23, Feb. 2013.

[7] O. Knecht, R. Bosshard, and J. W. Kolar, "High-efficiency transcutaneous energy transfer for implantable mechanical heart support systems," *IEEE Trans. Power Electron.*, vol. 30, no. 11, pp. 6221–6236, Nov. 2015.

[8] F. Musavi and W. Eberle, "Overview of wireless power transfer technologies for electric vehicle battery charging," *IET Power Electron.*, vol. 7, no. 1, pp. 60–66, Jan. 2014.

[9] S. Li, W. Li, J. Deng, T. D. Nguyen, and C. C. Mi, "A double-sided LCC compensation network and its tuning method for wireless power transfer," *IEEE Trans. Veh. Technol.*, vol. 64, no. 6, pp. 2261–2273, Jun. 2015.

[10] J. Zhang, X. Yuan, C. Wang, and Y. He, "Comparative analysis of two-coil and three-coil structures for wireless power transfer," *IEEE Trans. Power Electron.*, vol. 32, no. 1, pp. 341–352, Jan. 2017.

[11] S. Moon, B.-C. Kim, S.-Y. Cho, C.-H. Ahn, and G.-W. Moon, "Analysis and design of a wireless power transfer system with an intermediate coil for high efficiency," *IEEE Trans. Ind. Electron.*, vol. 61, no. 11, pp. 5861–5870, Nov. 2014.

[12] S. Bi, C. K. Ho, and R. Zhang, "Wireless powered communication: Opportunities and challenges," *IEEE Commun. Mag.*, vol. 53, no. 4, pp. 117–125, Apr. 2015.

[13] K. Huang and X. Zhou, "Cutting the last wires for mobile communications by microwave power transfer," *IEEE Commun. Mag.*, vol. 53, no. 6, pp. 86–93, Jun. 2015.

[14] W. H. Ko, S. P. Liang, and C. D. F. Fung, "Design of radio-frequency powered coils for implant instruments," *Med. Biol. Eng. Comput.*, vol. 15, no. 6, pp. 634–640, 1977.

[15] K. Wu, D. Choudhury, and H. Matsumoto, "Wireless power transmission, technology, and applications [scanning the issue]," *Proc. IEEE*, vol. 101, no. 6, pp. 1271–1275, Jun. 2013.

[16] A. Kurs, A. Karalis, R. Moffatt, J. D. Joannopoulos, P. Fisher, and M. Soljačić, "Wireless power transfer via strongly coupled magnetic resonances," *Science*, vol. 317, no. 5834, pp. 83–86, 2007.

[17] M. Kiani, B. Lee, P. Yeon, and M. Ghovanloo, "A Q-modulation technique for efficient inductive power transmission," *IEEE J. Solid-State Circuits*, vol. 50, no. 12, pp. 2839–2848, Dec. 2015.

[18] W. X. Zhong and S. Y. R. Hui, "Maximum energy efficiency tracking for wireless power transfer systems," *IEEE Trans. Power Electron.*, vol. 30, no. 7, pp. 4025–4034, Jul. 2015.

[19] W. Zhang and C. C. Mi, "Compensation topologies of high-power wireless power transfer systems," *IEEE Trans. Veh. Technol.*, vol. 65, no. 6, pp. 4768–4778, Jun. 2016.

[20] X. Tan and X. Ruan, "Equivalence relations of resonant tanks: A new perspective for selection and design of resonant converters," *IEEE Trans. Ind. Electron.*, vol. 63, no. 4, pp. 2111–2123, Apr. 2016.

[21] R.-F. Xue, K.-W. Cheng, and M. Je, "High-efficiency wireless power transfer for biomedical implants by optimal resonant load transformation," *IEEE Trans. Circuits Syst. I, Reg. Papers*, vol. 60, no. 4, pp. 867–874, Apr. 2013.

[22] C.-J. Chen, T.-H. Chu, C.-L. Lin, and Z.-C. Jou, "A study of loosely coupled coils for wireless power transfer," *IEEE Trans. Circuits Syst. II, Exp. Briefs*, vol. 57, no. 7, pp. 536–540, Jul. 2010.

[23] A. Qusba, A. K. RamRakhyani, J.-H. So, G. J. Hayes, M. D. Dickey, and G. Lazzi, "On the design of microfluidic implant coil for flexible telemetry system," *IEEE Sensors J.*, vol. 14, no. 4, pp. 1074–1080, Apr. 2014.

[24] E. S. G. Rodríguez, A. K. RamRakhyani, D. Schurig, and G. Lazzi, "Compact low-frequency metamaterial design for wireless power transfer efficiency enhancement," *IEEE Trans. Microw. Theory Techn.*, vol. 64, no. 5, pp. 1644–1654, May 2016.

[25] E. S. G. RodrÃguez, M. Machnoor, and G. Lazzi, "On the generation of nondiffracting beams in extremely subwavelength applications," *IEEE Trans. Antennas Propag.*, vol. 65, no. 10, pp. 5228–5237, Oct. 2017.

[26] P. Kosta *et al.*, "Electromagnetic safety assessment of a cortical implant for vision restoration," *IEEE J. Electromagn., RF, Microw. Med. Biol.*, vol. 2, no. 1, pp. 56–63, Mar. 2018.

[27] *IEEE Standard for Safety Levels With Respect to Human Exposure to Radio Frequency Electromagnetic Fields, 3 KHz to 300 GHz*, IEEE Standard C95.1-2005 (Revision of IEEE Std C95.1-1991), Apr. 2006, pp. 1–238.

[28] S. Gabriel, R. W. Lau, and C. Gabriel, "The dielectric properties of biological tissues: II. Measurements in the frequency range 10 Hz to 20 GHz," *Phys. Med. Biol.*, vol. 41, no. 11, p. 2251, 1996.

[29] S. Y. R. Hui, W. Zhong, and C. K. Lee, "A critical review of recent progress in mid-range wireless power transfer," *IEEE Trans. Power Electron.*, vol. 29, no. 9, pp. 4500–4511, Sep. 2014.

[30] X. L. Chen *et al.*, "Human exposure to close-range resonant wireless power transfer systems as a function of design parameters," *IEEE Trans. Electromagn. Compat.*, vol. 56, no. 5, pp. 1027–1034, Oct. 2014.

[31] M. Van Paemel, "High-efficiency transmission for medical implants," *IEEE Solid-State Circuits Mag.*, vol. 3, no. 1, pp. 47–59, Jan. 2011.

[32] A. K. RamRakhyani and G. Lazzi, "Multicoil telemetry system for compensation of coil misalignment effects in implantable systems," *IEEE Antennas Wireless Propag. Lett.*, vol. 11, pp. 1675–1678, 2012.

[33] W. X. Zhong, C. Zhang, X. Liu, and S. Y. R. Hui, "A methodology for making a three-coil wireless power transfer system more energy efficient than a two-coil counterpart for extended transfer distance," *IEEE Trans. Power Electron.*, vol. 30, no. 2, pp. 933–942, Feb. 2015.

[34] A. M. Sodagar, K. D. Wise, and K. Najafi, "A wireless implantable microsystem for multichannel neural recording," *IEEE Trans. Microw. Theory Techn.*, vol. 57, no. 10, pp. 2565–2573, Oct. 2009.

[35] R. R. Harrison *et al.*, "A low-power integrated circuit for a wireless 100-electrode neural recording system," *IEEE J. Solid-State Circuits*, vol. 42, no. 1, pp. 123–133, Jan. 2007.

[36] S. B. Lee, H.-M. Lee, M. Kiani, U.-M. Jow, and M. Ghovanloo, "An inductively powered scalable 32-channel wireless neural recording system-on-a-chip for neuroscience applications," *IEEE Trans. Biomed. Circuits Syst.*, vol. 4, no. 6, pp. 360–371, Dec. 2010.

[37] L. Karumbaiah *et al.*, "Relationship between intracortical electrode design and chronic recording function," *Biomaterials*, vol. 34, no. 33, pp. 8061–8074, Nov. 2013.

[38] G. McConnell, H. Rees, A. Levey, C. Gutekunst, R. Gross, and R. Bellamkonda, "Implanted neural electrodes cause chronic, local inflammation that is correlated with local neurodegeneration," *J. Neural Eng.*, vol. 6, p. 056003, Oct. 2009.

[39] X. Liu, W. M. Ng, C. K. Lee, and S. Y. Hui, "Optimal operation of contactless transformers with resonance in secondary circuits," in *Proc. 23rd Annu. IEEE Appl. Power Electron. Conf. Expo.*, Feb. 2008, pp. 645–650.

[40] D. Ahn and S. Hong, "A study on magnetic field repeater in wireless power transfer," *IEEE Trans. Ind. Electron.*, vol. 60, no. 1, pp. 360–371, Jan. 2013.

[41] A. K. RamRakhyani and G. Lazzi, "Multi-coil approach to reduce electromagnetic energy absorption for wirelessly powered implants," *Healthcare Technol. Lett.*, vol. 1, no. 1, pp. 21–25, 2014.

Manjunath Machnoor (S'16) received the B.Eng. degree in electronics and communications from the RNS Institute of Technology, Bengaluru, India, in 2011, and the M.Tech. degree in electronic systems from the Department of Electronic Systems and Engineering, Indian Institute of Science, Bengaluru, in 2013. He is currently pursuing the Ph.D. degree in electrical engineering with the University of Southern California, Los Angeles, CA, USA.

He was an ASIC IC Design Engineer Staff I at Broadcom Telecommunications Pvt. Ltd., Bengaluru, from 2013 to 2014, and a Project Associate with the Microwave Laboratory, Electrical and Communication Engineering Department, Indian Institute of Science, from 2014 to 2016. His current research interests include wireless power transfer for electric vehicles and biomedical devices.

Erik Saturnino Gámez Rodríguez (M'17) was born in El Rosario, Cuscatlán, El Salvador. He received the bachelor's degree and the M.Sc. and Ph.D. degrees in electrical engineering from The University of Utah, Salt Lake City, UT, USA.

His current research interests include wireless power transfer optimization and enhancement, ultra-wideband antenna design and miniaturization, active antennas, novel wireless communication devices, radar imaging, and applications of spatial filtering in the microwave regime.

Pragya Kosta (S'15) received the B.Tech. degree in electronics and communication engineering from IIT Jabalpur, Jabalpur, India, in 2010, and the M.Tech. degree in electronics and communication engineering from IIT Roorkee, Roorkee, India, in 2012. She is currently pursuing the Ph.D. degree in electrical and computer engineering with The University of Utah, Salt Lake City, UT, USA.

From 2012 to 2015, she was an Assistant Professor with the Department of Electronics and Communication Engineering, Maharana Pratap Group of Institutions, Kanpur, India, and the CMR Institute of Technology, Bengaluru, India. She has previous research experience in the fields of computational electromagnetics and antenna design. Her current research interests include computational modeling for neural stimulation, neuroprostheses, implantable devices, and bioelectromagnetics.

John Stang, photograph and biography not available at the time of publication.

Gianluca Lazzi (S'94–M'95–SM'99–F'08) received the Dr.Eng. degree in electronics from the University of Rome La Sapienza, Rome, Italy, in 1994, the Ph.D. degree in electrical engineering from The University of Utah, Salt Lake City, UT, USA, in 1998, and the Executive M.B.A. degree, specialized in corporate finance, from the IE Business School, Madrid, Spain, in 2015.

He was a Professor from 2006 to 2009, an Associate Professor from 2003 to 2006, and an Assistant Professor from 1999 to 2003 with the Department of Electrical and Computer Engineering, North Carolina State University, Raleigh, NC, USA. He served as a USTAR Professor and the Department Chair of the Department of Electrical and Computer Engineering, The University of Utah, where he was also the Director of the Engineering Entrepreneurship Certificate. In 2015, he co-founded Teveri LLC, Salt Lake City, UT, USA, which is focused on the commercialization of liquid metal technology for textile and consumer electronics applications. He is currently a Provost Professor of ophthalmology, electrical engineering, and clinical entrepreneurship at the University of Southern California, Los Angeles, CA, USA. He has authored or co-authored more than 200 international journal papers, conference presentations, and book chapters on implantable devices, medical applications of electromagnetics, wireless telemetry, antenna design, computational modeling, dosimetry, and bioelectromagnetics.

Dr. Lazzi was a recipient of the 1996 Curtis Carl Johnson Memorial Award for the best student paper presented at the 18th Annual Technical Meeting of the Bioelectromagnetics Society, the 1996 URSI Young Scientist Award, the 2001 Whitaker Foundation Biomedical Engineering Grant for Young Investigators, the 2001 National Science Foundation CAREER Award, the 2003 NCSU Outstanding Teacher Award, the 2003 NCSU Alumni Outstanding Teacher Award, the 2003 ALCOA Foundation Engineering Research Award, the 2006 H.A. Wheeler Award from the IEEE Antennas and Propagation Society for the best application paper published in the IEEE TRANSACTIONS ON ANTENNAS AND PROPAGATION in 2005, the 2008 Best Paper Award at the IEEE GLOBECOM Conference, the 2009 ALCOA Foundation Distinguished Engineering Research Award, the 2009 R&D 100 Award, and the 2009 Editors' Choice Award from the R&D Magazine for the Artificial Retina Project. He was the Chair of the Commission K—Electromagnetics in Biology and Medicine from 2006 to 2008 and a Member-at-Large of the U.S. National Committee of the International Union of Radio Science (URSI) from 2009 to 2011. In 2014, he was the General Co-Chair of the IEEE Microwave Symposium on RF and Wireless Technologies for Biomedical Applications. He was an Associate Editor for the IEEE ANTENNAS AND WIRELESS PROPAGATION LETTERS from 2001 to 2007 and served as the Editor-in-Chief for the IEEE ANTENNAS AND WIRELESS PROPAGATION LETTERS from 2008 to 2013. He also served as a Guest Editor for the Special Issue on Biological Effects and Medical Applications of RF/Microwaves of the IEEE TRANSACTIONS ON MICROWAVE THEORY AND TECHNIQUES in 2004 and the Technical Program Chair of the IEEE Antennas and Propagation International Symposium and the URSI Meeting in Charleston, SC, USA, in 2009. He served as a member of the Editorial Board of the PROCEEDINGS OF THE IEEE, the Chair of the IEEE Sensors Council Fellow Committee, and the Chair of the Publications Committee of the IEEE AP Society. He currently serves as the VP Publications of the IEEE Sensors Council and a member of the Editorial Board of the IEEE ACCESS.